Solid State Phenomena
ISSN: 1662-9779, Vol. 391, pp 29-42
doi:10.4028/p-aFH2MU

Submitted: 2025-12-18
Revised: 2026-02-21
Accepted: 2026-02-23
Online: 2026-04-20

Preliminary Comparative Assessment of Hole Quality and Geometrical Tolerances in AM-Built and CNC-Drilled PLA Components

Martina Panico[1,a*], Guido Di Bella[2,b], Massimo Durante[1,c], Mohamed Chairi[2,3,d], Antonio Langella[1,e] and Luca Boccarusso[1,f]

[1]Dept. of Chemical, Materials and Production Engineering, University of Naples "Federico II", P.le Tecchio 80, 80125, Naples, Italy

[2]Department of Engineering, University of Messina, Contrada di Dio, 98166 Messina, Italy

[3]CNR ITAE, Salita S. Lucia sopra Contesse 5, 98126 Messina, Italy

[a*]martina.panico@unina.it, [b]guido.dibella@unime.it, [c]mdurante@unina.it, [d]mohamedchairi@cnr.it, [e]antgella@unina.it, [f]luca.boccarusso@unina.it

Keywords: Fused Deposition Modelling (FDM), Hole Quality, CNC Drilling, AM-Built Holes.

Abstract. The increasing adoption of polymer additive manufacturing (AM) in functional applications has intensified the need for reliable hole-making strategies, particularly when printed components require mechanical fastening or post-processing. However, the layered architecture of fused-filament fabrication (FFF) parts typically leads to dimensional inaccuracy and thermally induced defects during drilling. This study examines the quality of holes made directly with FFF technology and those obtained through traditional drilling on polylactic acid (PLA) components produced with two different layer heights (0.20 and 0.28 mm). Additively manufactured holes were analysed via least-squares circle fitting and roundness evaluation, revealing high repeatability but substantial undersizing (>1 mm deviation from the 6.35 mm nominal diameter). CNC drilling tests were then performed under a full-factorial combination of spindle speed and feed rate, assessing thrust force, torque, infrared-based cutting temperature, and burr formation for both top and bottom sample side. Results show that CNC drilling can restore near-nominal dimensional accuracy, but only within a restricted process parameters window. Low feed rates promote severe thermal-viscoplastic deformation, while specific combinations of spindle speed and entry surface strongly influence burr formation.

Introduction

Additive manufacturing (AM) is progressively extending its application domain from rapid prototyping to the production of structural and functional components for industrial use [1,2]. The increasing maturity of polymer-based additive processes, especially those relying on Fused Filament Fabrication (FFF) [3], has enabled the fabrication of lightweight and customized geometries with reduced material waste and shortened lead time. Despite these advantages, AM still faces significant limitations when strict geometric tolerances and performance requirements must be met, particularly in scenarios where the manufactured components are subjected to assembly operations or load-bearing conditions [4–6]. In such cases, even small deviations in local features, such as dimensional accuracy or surface integrity of holes, can critically affect mechanical performance, functional fitting and long-term reliability of the joined structures.

Holes represent a key design feature, especially in components destined for assembly via mechanical fastening. In conventional manufacturing chains, hole production is typically performed through drilling, allowing accurate control of positioning, dimensional tolerance and surface quality. Conversely, in AM, holes can be directly generated during the layer-by-layer deposition process, potentially eliminating secondary machining operations. While this approach is attractive in terms of production time and sustainability, literature highlights that printed holes often suffer from dimensional inaccuracy, poor surface finish, a higher tolerance variability due to staircase effects, process-induced defects, and accumulation of anisotropic printing deviation [7–9]. Nevertheless, AM-built holes may avoid the localized thermal and mechanical stresses associated with CNC

drilling, representing a potential advantage in terms of reduced burr formation and mitigation of heat-affected or plastically deformed regions [10,11].

Previous studies have predominantly focused on the dimensional deviations induced by AM at component scale, whereas only limited work has systematically addressed the comparison between holes fabricated directly via AM and those produced through drilling on AM-built substrates. In particular, recent investigations have examined drilling performance on 3D-printed PLA in terms of thrust force, torque and surface integrity, but without benchmarking these outcomes against the characteristics of AM-built holes [11,12]. Furthermore, little attention has been paid to the influence of drilling parameters on post-process geometrical tolerances in additively manufactured polymers, nor to the assessment of positional repeatability, an aspect that is essential in applications where multi-part alignment or functional integration is required. This gap hinders the definition of reliable design criteria for integrating AM with conventional machining, especially for assembly-critical component or hybrid process chains.

In this context, the present work proposes a comparative experimental investigation on the quality of holes fabricated during the AM process or via CNC drilling after deposition phase. PLA plates were produced via FFF using two distinct values of layer thickness (0.20 mm and 0.28 mm), and two configurations were examined: (i) specimens containing a row of AM-built holes, and (ii) full-solid specimens subsequently drilled under different combinations of rotational speed and feed rate. CNC drilling tests were also performed by varying the material entry surface, distinguishing between the top layer (T-side) and the surface directly in contact with the printing bed (B-side), in order to assess the influence of print-induced surface morphology and process-induced microstructural anisotropy on drilling response. Hole quality was assessed in terms of dimensional accuracy, geometrical and positional tolerances, as well as surface features and burr height, while drilling process monitoring included thrust force, torque and temperature evolution. Based on the experimental outcomes, the optimal drilling condition was identified and employed to replicate a sequence of drilled holes for direct comparison with AM-built ones. Therefore, the objective of this study is to quantitatively evaluate the limitations and opportunities associated with both fabrication strategies, providing useful insights for integrating AM and drilling technologies in functional polymer components and supporting their potential deployment in assembly-critical applications.

Materials and Methods

PLA specimens with nominal dimensions of 200 mm × 30 mm × 3.2 mm were manufactured via Fused Filament Fabrication (FFF) using two layer thickness configurations, namely 0.20 mm (PLA_020) and 0.28 mm (PLA_028). A commercial black PLA filament (PLA Basic, Filament2Print, Spain; 1.75 mm diameter, density 1.24 g/cm³, 1 kg spool) was employed for all prints. Printing was carried out at nozzle and bed temperatures within the ranges recommended by the manufacturer (190–230 °C and 50–70 °C, respectively). For each layer condition, two sets of samples were produced: the first consisting of specimens with holes directly integrated during the AM process with a nominal diameter of 6.35 mm and a centre-to-centre spacing of 12.7 mm. Each AM-drilled specimen incorporated a sequence of 15 holes, and three specimens were fabricated per layer configuration, resulting in a total of 45 integrated holes for PLA_020 and 45 for PLA_028. The second set comprised solid specimens intended for subsequent CNC drilling. The printing process was performed using Bambu Lab A1 3D printer, maintaining identical build orientation and tool path strategy for all tests; all process parameters (e.g., nozzle temperature, print speed, bed temperature, infill strategy, cooling conditions) were held constant and are summarized in Table 1.

Table 1 Parameters of 3D printing process.

Parameter	Value/Description
Printing technology	Fused Filament Fabrication (FFF)
Printer model	Bambu Lab A1
Nozzle diameter	0.4 mm
Nozzle temperature	220 °C
Bed temperature	65 °C
Layer thickness	0.20 mm / 0.28 mm
Build orientation	Flat, XY-plane
Walls / Shells	2 loops
Infill density	100%
Infill pattern	Rectilinear
Infill direction	45°
Infill-to-wall overlap	15%
Initial layer speed (walls)	50 mm/s
Initial layer speed (infill)	105 mm/s
Print speed – external wall	200 mm/s
Print speed – internal wall	300 mm/s
Print speed – infill	270 mm/s
Cooling	Active cooling after first layers

CNC drilling tests were performed in dry conditions on a five-axis machining centre (C.B Ferrari, Italy), according to a full-factorial parameter matrix combining different levels of spindle rotation and feed rate. The selected levels for the spindle speed were 800 rpm, 1600 rpm, and 2400 rpm, while the corresponding values for the feed rate were 0.01 mm/rev, 0.05 mm/rev, and 0.1 mm/rev. Based on the evidence reported in the literature [11,12], these cutting parameters were selected with the aim of exploring a sufficiently wide process window. In this case, the feed range (0.01 – 0.10 mm/rev) vary from a condition characterised by high contact time and greater compressive interaction between the tool and the material, to more aggressive values, where chip formation and evacuation are facilitated. At the same time, the spindle speed levels (800-2400 rpm, corresponding to a cutting speed of approximately 16-48 m/min) cover a transition from conservative low-heat conditions to high-energy regimes, where the effects of thermal softening become increasingly significant. All CNC tests were performed using a conventional HSS twist drill bit with a diameter of 6.35 mm and a point angle of 140° (supplied by HTT High Tech Tools, Italy). For each condition, three holes were drilled. As an additional experimental variable, the entry surface for drilling was varied to capture the influence of deposition-induced surface characteristics. Specifically, drilling was performed from both the top surface (last deposited layer side, T-side) and the bottom surface (in contact with the printing bed, B-side), which exhibit different thermal histories and surface conditions. Surface roughness measurements, conducted by using a Confocal microscope (Sensofar S neox, 20x magnification) on an area of 25 mm^2, highlighted that PLA_020 samples has an S_a of 8.415 µm (top) and 21.770 µm (bottom), while PLA_028 samples has values of 7.860 µm (top) and 20.114 µm (bottom), confirming that the bed-side layers are significantly rougher and potentially more affected by build-induced irregularities. In addition, the first layer deposited, in order to promote adhesion to the printing plate, has a height of 0.30 mm (regardless of the design height of the layers). Process monitoring included thrust force and torque acquisition using a 6-axis force/torque sensor (model K-MCS10, HBK World, Southfield, MI, USA) positioned between the workpiece and machine table, with a sampling frequency of 1200 Hz, whereas thermal data were collected during selected trials for qualitative assessment of heat generation during chip evacuation. The experimental setup is shown in Fig. 1. Additionally, infrared thermal imaging was acquired using an Avio R300SR infrared camera on a subset of drilling tests, specifically for selected spindle speed–feed rate combinations where significant thermal effects were expected. The emissivity was set to 0.95, consistent with typical values for opaque thermoplastic polymers such as PLA. Thermal images were recorded at a frame

rate of 60 Hz. The monitored wavelength range was centred at approximately 10 µm within the long-wave infrared region. The camera was oriented to directly observe the hole entry surface (tool entry side) throughout the drilling process.

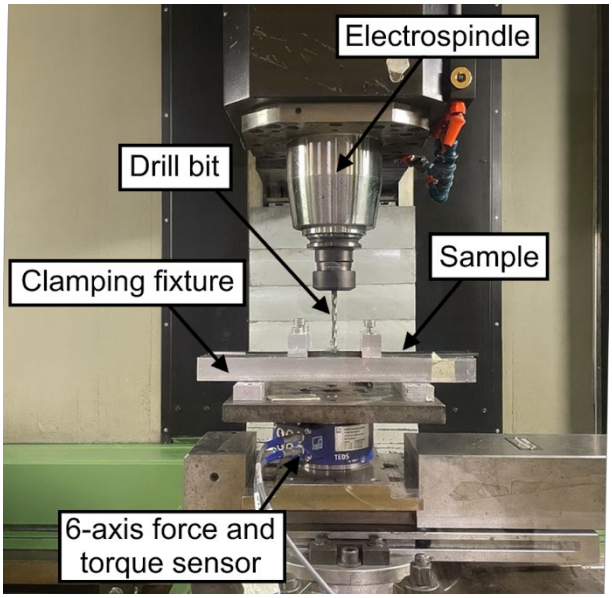

Fig.1. Experimental drilling setup.

The hole quality of both CNC drilled and additively pre-integrated holes was evaluated through multiple metrics. For drilled hole, burr height was measured by non-contact 3D optical profiling using a confocal microscope (Sensofar, S, 20x magnification), scanning the entire hole circumference and extracting the maximum burr height as the peak out-of-plane deviation from the original surface [13,14]. Roundness, for both drilled and AM-built holes, was assessed using a Zeiss DuraMax coordinate measuring machine (CMM) with a 1 mm spherical touch probe, programmed via Zeiss Calypso software to ensure repeatable measurement routines [13,14]. For each hole, the probe was initially centred on the nominal hole axis and subsequently acquired 400 discrete measurement points along the circumference at mid-depth of the hole, following a clockwise path. The acquired coordinates were processed through least-squares circle (LSC) fitting to determine the best-fitting diameter. Maximum and minimum local diameters were also extracted to calculate the roundness error ($D_{max} - D_{min}$), in accordance with ISO 12181. Fig. 2 shows the procedure carried out.

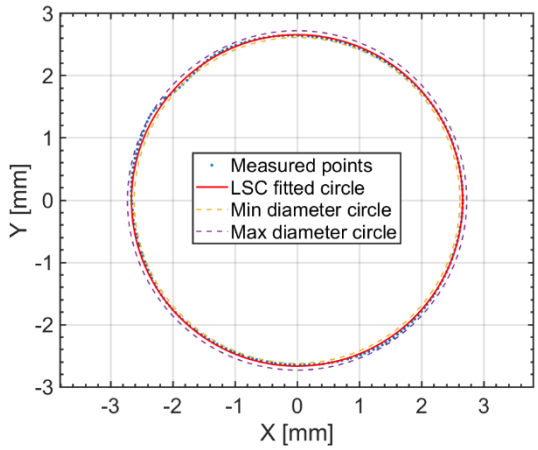

Fig.2. Example of roundness assessment.

The experimental workflow can therefore be summarised as follows: specimen fabrication via FFF for both layer thicknesses, CNC drilling according to parameter matrix and entry surface variation, process monitoring (force, torque and thermography where applicable), and post-process assessment

of hole quality including dimensional, geometrical and surface-related indicators for comparison between AM-built and CNC-drilled holes.

Results and Discussion

Analysis of CNC-drilled holes. For illustrative purpose, Fig. 3 reports the evolution of thrust force (a) and torque (b) for the representative drilling condition at $n = 1600$ rpm and $f = 0.05$ mm/rev. Similar to the trends observed across all tested combinations of process parameters, no substantial differences were detected in the shape of thrust force, torque profiles and their peak values when varying either the entry surface (top versus bottom) or the layer thickness (0.20 mm versus 0.28 mm). A further observation can be made regarding the evolution of the torque signal after the maximum peak, particularly in the phase leading to complete tool exit. For B-side drilling, for both investigated layer heights, the post-peak decay does not follow a monotonic trend toward zero. Instead, once the torque has dropped to approximately half of its maximum value, the signal enters a temporary plateau whose duration depends on the process parameters. This plateau precedes the final collapse to zero. A cautious interpretation of this behaviour may relate to the intrinsic structure of the last deposited layer: when drilling from the B-side, the tool eventually engages what corresponds to the topmost printing layer, characterized by a continuous morphology for mainly aesthetic reasons, which may temporarily provide an additional resistance to penetration, thereby sustaining the torque at an intermediate level before full breakthrough.

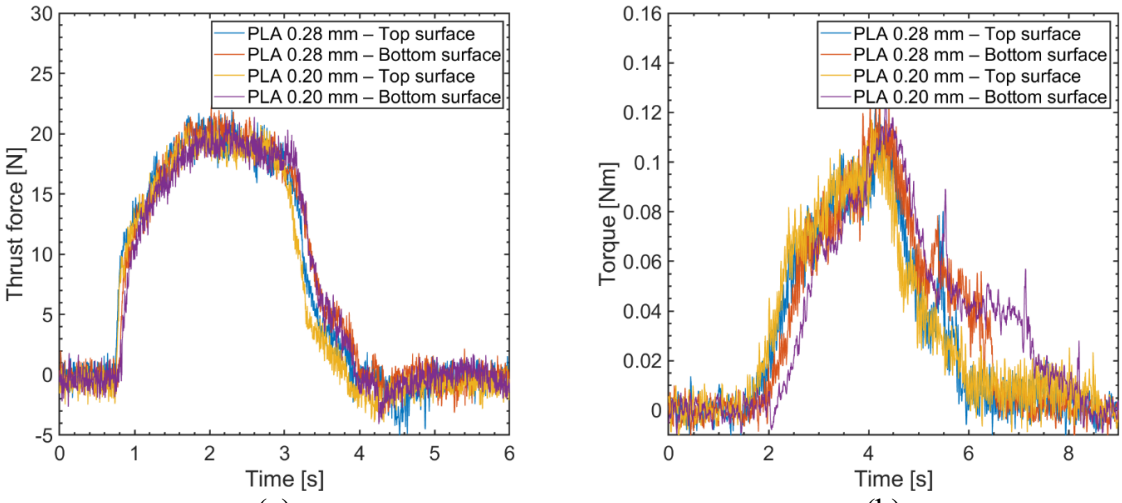

(a) (b)

Fig. 3. Time evolution of thrust force (a) and torque (b) during CNC drilling of PLA specimens under different layer thickness and entry surface configurations.

As shown in Fig. 4a and Fig. 4b, the feed rate plays the dominant role in determining the peak thrust force. Notably, $f = 0.01$ mm/rev leads to the highest force values for all spindle speeds and both entry conditions. This behaviour is attributed to the extremely reduced thickness of the uncut chip, which limits the efficiency of chip formation. The material remains in contact with the cutting edges for a longer time, causing greater mechanical compression and greater local friction, whit a consequent increase in thrust force. Under such conditions, a clear increasing trend with rotational speed can be observed. Such trend aligns with the thermos-sensitive behaviour of PLA. While increasing spindle speed generally promotes cutting temperature and, consequently, material softening (leading to a reduction of resistance to penetration), two concurrent effects may arise at higher speeds. On one side, the increase in strain rate may enhance the material's apparent stiffness, counterbalancing softening to some extent and resulting in slightly higher force levels. On the other side, when the local thermal input exceeds a critical threshold, the polymer transitions from viscoplastic state to a semi-fluid condition. In this regime, the material trends not to fracture or detach cleanly under the cutting action but rather undergoes local deformation and smearing around the tool edges. This behaviour hinders efficient chip formation and increases the energy required for material

displacement, which may lead to local increases in cutting forces despite the nominal thermal softening. No substantial differences emerged between T-side and B-side drilling entries. The two layer thickness configurations generally exhibit comparable thrust force levels, with only marginal differences except at the lowest feed rate (0.01 mm/rev). In this specific condition, the specimens printed with 0.28 mm layer height showed higher peak values compared to those produced with 0.20 mm. As shown in Fig. 4c and Fig. 4d, torque presents a progressive increment with spindle speed up to 1600 rpm, followed by a stabilisation or slight decrease at 2400 rpm. This behaviour reflects the combined effect of strain rate stiffening and thermally induced softening of PLA. At low feed rate (0.01 mm/rev), torque values remain limited due to reduced chip thickness and deformation-dominant removal mechanisms, while the highest torque levels are recorded at $f = 0.1$ mm/rev, where chip formation becomes more efficient and the cutting plane area increases. Only marginal differences emerge between the two layer heights, except at the lowest feed setting, where the coarser stratification of PLA_028 favours local softening and results in slightly lower torque peaks.

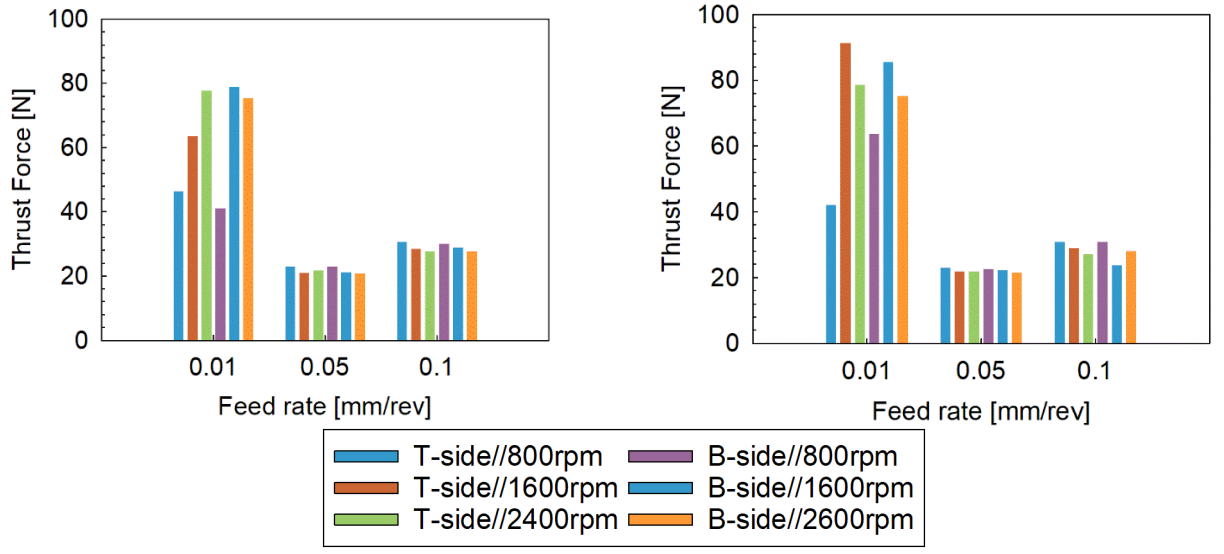

(a) – 0.20 mm (b) – 0.28 mm

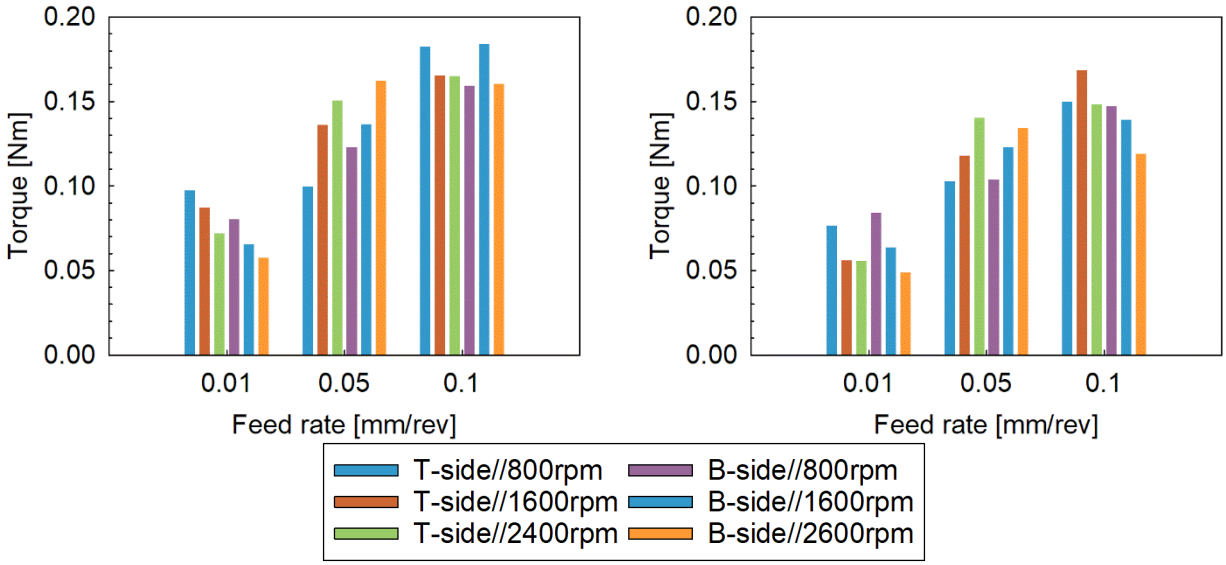

(c) – 0.28 mm (d) – 0.28 mm

Fig. 4. (a, b) Maximum thrust force with increasing feed rate for the investigated spindle speeds and drilling direction, for (a) PLA specimens printed with 0.20 mm layer height and (b) PLA specimens printed with 0.28 mm layer height. (c, d) Corresponding maximum torque trends under the same drilling conditions.

In order to better understand the influence of thermos-mechanical interaction on drilling response, thermographic monitoring was performed for selected combinations of process parameters, i.e., those expected to generate significant temperature rise based on the thrust force and torque analysis. Representative results are reported in Fig. 5, which shows the surface temperature distribution and corresponding temperature profile extracted along a horizontal section passing through the hole centre for the 2400 rpm – 0.10 mm/rev combination. Under these conditions, the temperature peak reached approximately 54.5 °C. When analysing the combined effect of spindle speed and feed rate, a clear thermal trend emerges. At 0.01 mm/rev, surface temperatures increased from 59°C (800 rpm) to 68.6°C (1600 rpm), reaching 87.2°C at 2400 rpm, in agreement with the observed rise in thrust force. In this configuration, the extremely thin chip promotes prolonged contact between the tool and the workpiece, enhancing friction and heat generation while limiting heat evacuation via material removal. As torque remains relatively low due to inefficient chip formation, most of the generated heat is dissipated into the hole walls, resulting in a strong increase of temperature. Conversely, at 2400 rpm with increasing feed rate (0.01, 0.05, 0.1 mm/rev), peak temperatures gradually decreased from 87.2°C to 70.8°C and finally to 54.5°C, despite the corresponding rise in torque. This behavior is consistent with the finding that as the thickness of the uncut chip increases, material removal per revolution becomes more effective, allowing the chip to play a key role in heat evacuation. In addition, the reduced exposure time of the material to the cutting edge limits local heat accumulation, preventing excessive softening. These observations align with the dual response of PLA to thermomechanical loading. At low chip thickness, the combination of low material removal rate (MRR, volume of material removed per time unit) and prolonged local deformation leads to notable heating and increased thrust force, exacerbated by viscoelastic deformation of the softened polymer. At higher feed rates, the process transitions towards a chip-forming regime with improved energy distribution, thereby reducing thermal input at the cutting interface despite the higher torque required for thicker chip deformation.

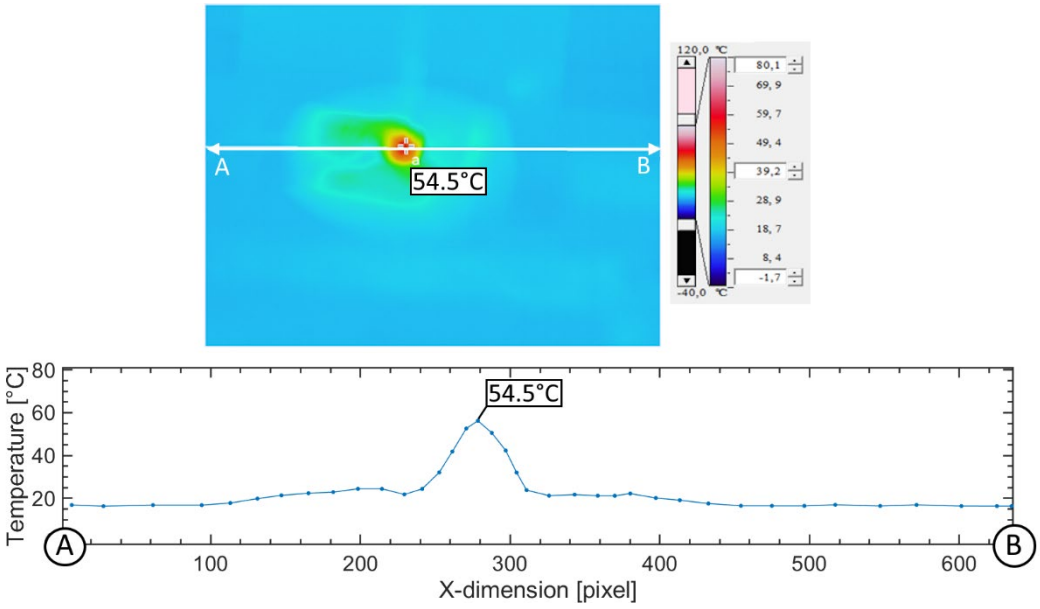

Fig. 5. Thermographic analysis of the PLA drilling process under the 2400 rpm – 0.10 mm/rev combination.

Fig. 6 illustrates the evolution of burr height at the hole entry as a function of feed rate and spindle speed for specimens manufactured with 0.20 mm layer height, distinguishing between drilling from the extrusion surface (T-side) and from the build-plate contact surface (B-side). At f = 0.01 mm/rev, burr height progressively increases from 239 µm at 800 rpm to 463 µm at 1600 rpm, reflecting the combined action of increased thrust force and temperature measured at the tool entry section. At 2400 rpm, the burr height appears to decrease to 159 µm; however, visual inspection confirms the presence of severe local edge rounding (‘chamfer-like’ deformation, see Fig. 7a), indicating that the

reduced measured value is the result of material ejection rather than actual burr minimisation (for this reason, the burr height data of 159 μm is not shown in Fig. 6). This condition is associated with the highest heat input (cutting temperatures previously measured up to 87.2 °C), which causes extensive lateral deformation of the material. At an intermediate feed rate (f = 0.05 mm/rev), the burr height decreases at 800 rpm (208 μm) but remains high at 1600 rpm (346 μm). At 2400 rpm, chip accumulation was observed around the edge of the hole (>> 1 mm), making quantitative measurement of the burr meaningless (see Fig. 7b). This can be attributed to an unfavourable combination of increased chip thickness, exceeding the glass transition temperature of PLA, and limited chip evacuation, which favours local adhesion rather than fracture-based removal. At f = 0.10 mm/rev, the lowest values are recorded at 800 and 2400 rpm (90 μm and 109 μm respectively), with a pronounced peak at 1600 rpm (383 μm). The high-speed reduction of the spindle is associated with lower cutting temperatures (around 55 °C) that fall below the viscoplastic regime, restoring a more efficient chip formation mechanism.

When drilling from the surface in contact with the printing bed, both magnitude and morphology of burr formation change significantly. At f = 0.01 mm/rev, the burr height reaches 307 μm at 800 rpm (+28.39% compared to the burr measured for the B-side case), while at 1600 and 2400 rpm the adhesion of chips to the edge of the hole renders the measurement meaningless. At f = 0.05 mm/rev, the burr height is limited to 236 μm at 800 rpm but exceed 1 mm at 1600 rpm and return to chip adhesion at 2400 rpm. This highlights that the choice of entry surface (as well as the surface finish and thickness) becomes critical when the cutting temperature exceeds the polymer transition range, while the chip thickness is sufficient to determine lateral friction. At f = 0.10 mm/rev, a general downward trend is observed as the rotation speed increases: from 184 μm (800 rpm) to 174 μm (1600 rpm) and down to 106 μm at 2400 rpm, closely matching the minimum values measured for T-side configuration under the same conditions. This is consistent with the decrease observed in the cutting temperature at 2400 rpm, which restores an effective chip cutting regime.

Unlike entry-side behaviour, no consistent trend was observed for burr height at hole exit, with severe burr occurrences spread across different parameter combinations. As shown by the qualitative observations, under the most critical conditions (as well as at minimum feed rate), the material did not generate a conventional burr but formed an accumulation that replicated the geometry of the tool tip (see Fig. 7c, 800 rpm – 0.01 mm/rev). This indicates sever localised softening and compressive flow of the PLA, with the material being plastically displaced around the drill tip without effective fracture propagation. Under these conditions, the polymer transitions to a semi-fluid state due to prolonged contact at low feed and high compressive stress, leading to stagnation and moulding of the material rather than chip separation induced by cutting. At intermediate feed (0.05 mm/rev), burr formation at the hole exit remains significant for both drilling entry configurations, particularly under low and medium spindle speeds. A substantial reduction is observed when increasing the spindle speed to 2400 rpm, where burr height decreases to 126.25 μm for T-side, corresponding to a reduction of approximately 12% compared with 1600 rpm, and to 106.10 μm for B-side, i.e. a reduction of approximately 89%. Although thermal measurements taken at the hole entrance indicate that local temperatures exceeded the glass transition threshold (approximately 70.8 °C), the shorter tool-material contact time at 2400 rpm limits plastic flow near the exit surface, thereby reducing the extent of deformation and material accumulation. Even when the feed rate increases to 0.10 mm/rev, in both T-side and B-side drilling configurations, there is a decrease in burr height as the rotation speed increases. However, at maximum rotation speed (2400 rpm), after the burr height decreases from 0.01 mm/rev to 0.05 mm/rev, it increases again to 0.10 mm/rev. This non-monotonic behaviour at high rotational speeds confirms that burr formation is determined by the combined effect of thermal and mechanical loads. Infrared measurements at the hole inlet showed that, for PLA_020 at 2400 rpm, the surface temperature decreases when the feed rate is increased from 0.05 to 0.10 mm/rev (from approximately 72 °C to approximately 55 °C), moving away from the peak thermal softening regime. However, the thrust force increases simultaneously at f = 0.10 mm/rev, leading to a more severe mechanical load during penetration. Under these conditions, the reduced dwell time of the tool in the material limits a further increase in temperature, but the increased penetration force promotes

more intense plastic deformation, which ultimately results in new burr height growth below 2400 rpm for both feed directions.

The burr formation behaviour observed for PLA_028 follows the same qualitative trends already described for PLA_020 (see Fig. 6b). In both entry configurations (T-side and B-side), the lowest feed rate (0.01 mm/rev) results in the most severe burr formation, particularly at 1600 rpm, where burr height reaches 849 µm on the T-side. Conversely, higher feed rates (0.10 mm/rev) generally result in lower burr levels, in line with lower tool-material interaction. Although the general trend corresponds to that described for samples printed with a layer height of 0.20 mm, samples printed with a layer height of 0.28 mm consistently exhibit higher top burr height under comparable process conditions. For example, at 800 rpm and 0.01 mm/rev, PLA_028 T-side produces a burr height of 382.8 µm, compared to 239.5 µm for PLA_020 T-side, corresponding to an approximate increase of 60%. Similarly, at 0.05 mm/rev and 1600 rpm, the burr height in PLA_028 T-side reaches 507.9 µm, compared to 346.1 µm for PLA_020 T-side (+47%). This can be attributed to the fact that, at the exit of the hole, the layer directly affected by the cutting action is thicker in the case of PLA_028 and behaves as a single deformable block, rather than being defined by several thinner layers as in PLA_020. One softened locally, this larger volume layer tends to undergo plastic deformation and accumulate around the cutting edges, thus promoting more severe burr development. Similarly to PLA_020, no monotonic trend can be identified for the burr generated at the hole exit in PLA_028 as a function of either feed rate or spindle speed. In contrast to the entry burr, no substantial differences emerge in absolute terms between the two entry configurations.

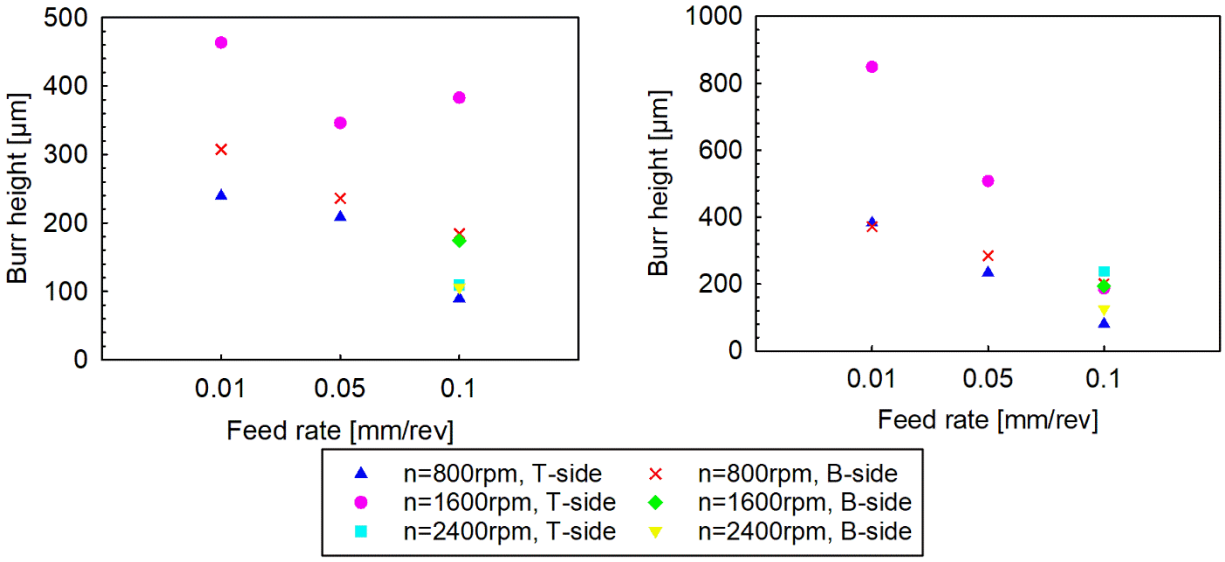

(a) (b)

Fig.6. Mean burr height measured at the hole entry as a function of feed rate and spindle speed for the two layer height configurations: (a) PLA_020 (0.20 mm layer height) and (b) PLA_028 (0.28 mm layer height).

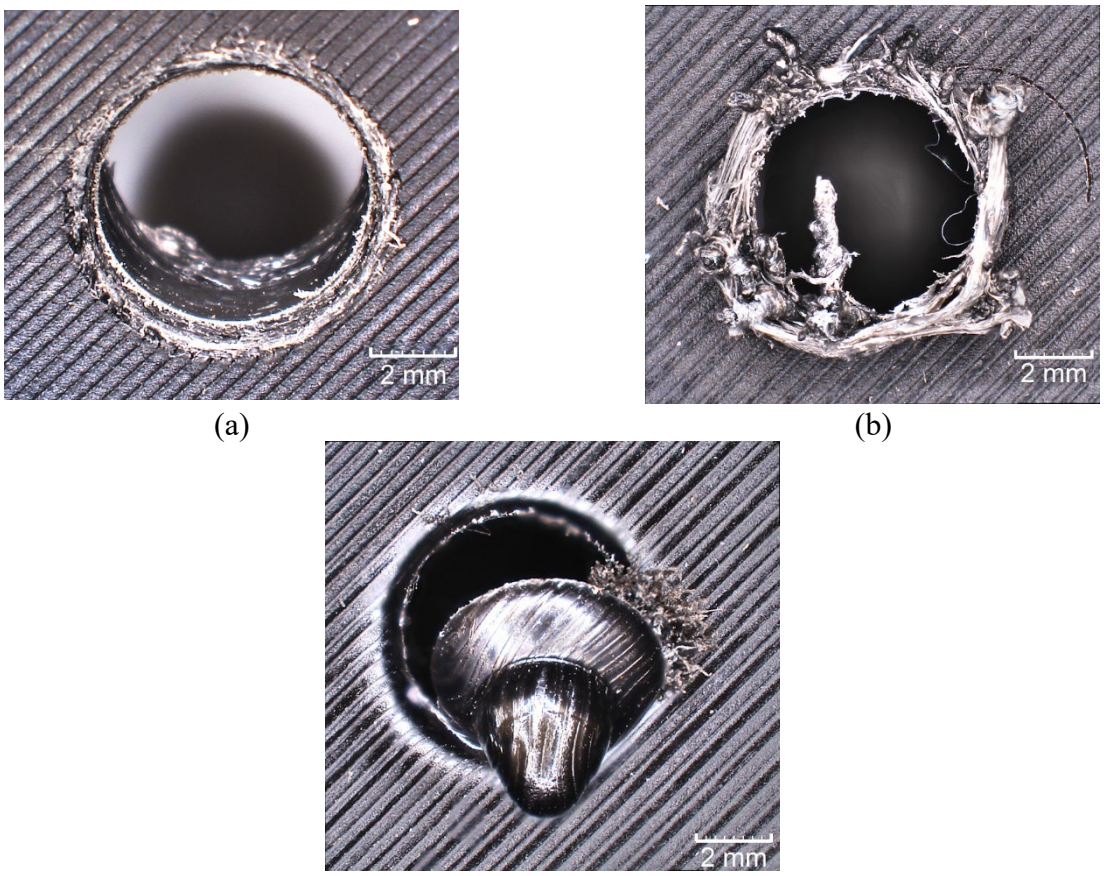

(a) (b)

(c)

Fig. 7. Representative images of burr formation under the most critical CNC drilling conditions: (a) 2400 rpm – 0.01 mm/rev (T-side); (b) 2400 rpm – 0.05 mm/rev (T-side) and (c) 800 rpm – 0.01 mm/rev.

The analysis of thrust force, torque, and burr formation reveals that the drilling response of FFF-printed PLA does not exhibit a single condition that simultaneously minimise all indicators. Instead, the results highlight the need for a process window-based approach. Across all configurations, the lowest thrust force values were obtained at an intermediate feed rate (0.05 mm/rev) combined with moderate-to-high spindle speeds (1600-2400 rpm). Lower feed levels (0.01 mm/rev) produced markedly higher forces due to deformation-dominated removal, whereas higher feed (0.10 mm/rev) increased the cutting load through a larger chip cross-section. Torque exhibited a distinct optimum. The lowest values consistently occurred at $f = 0.01$ mm/rev and $n = 2400$ rpm, but this condition cannot be considered optimal from a machining standpoint. As previously discussed, extremely low feed rates suppress chip formation and promote a deformation-dominated removal mechanism. In this regime, the cutting edges predominantly plough the material rather than producing a clean chip. This results in a reduction of torque (because the cutting engagement area is minimal) but at the expense of a severe increase in thrust force, extensive local plasticisation, poor evacuation of softened material, and pronounced burr formation. Burr height introduces an additional constraint that further refines the selection of suitable parameters. Across both layer heights (PLA_020 and PLA_028), the most favourable feed rates for burr minimisation lie in the interval $f = 0.05$–0.10 mm/rev. However, the preferred spindle speed differs depending on the drilling entry configuration. For T-side drilling, the lowest burr levels consistently occur at low spindle speeds (800 rpm), while for B-side drilling burr height is minimised under high-speed conditions (2400 rpm). Considering all performance indicators together, the most robust operating region for drilling FFF-printed PLA is defined by feed rates between 0.05 mm/rev and 0.10 mm/rev, combined with: low spindle speed (800 rpm) for T-side entry and high spindle speed (2400 rpm) for B-side entry.

Analysis of Additively Manufactured holes. The dimensional evaluation of the drilled AM holes was conducted by analysing the least-squares circle diameter (LSC), calculated on 45 holes for each layer configuration (PLA_020 and PLA_028). Statistical analysis showed that samples produced with 0.20 mm layer thickness exhibited an average LSC diameter of 5.311 mm with a standard deviation of 0.02056 mm, while 0.28 mm layer samples reported a mean value of 5.214 mm and a standard deviation of 0.01724 mm. To better evaluate dimensional repeatability, the coefficient of variation (CoV = σ/mean) was computed, resulting in 0.387% for PLA_020 and 0.331% for PLA_028. This indicates slightly more consistent dimensional performance when using the thicker layer. Fig. 8 reports the distribution of LSC diameter values through a histogram-based representation for both layer configurations. The PLA_020 configuration shows a marginally higher average diameter but also greater dispersion, whereas PLA_028 exhibits a more concentrated distribution, in agreement with statistical findings (lower CoV).

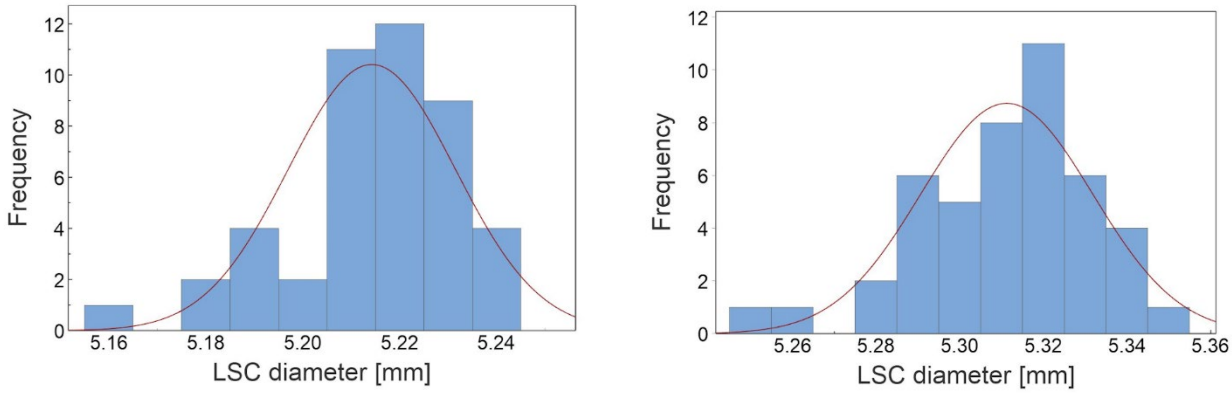

(a) (b)

Fig. 8. Distribution of the LSC diameter values measured on the as-printed holes for both layer thickness configurations: (a) PLA samples manufactured with 0.20 mm layer thickness, (b) PLA samples manufactured with 0.28 mm layer thickness.

Despite these differences, all measured diameters are well below the nominal design value of 6.35 mm, with average deviations of approximately -1.04 mm (PLA_020) and -1.14 mm (PLA_028). According to existing literature [15–17], this dimensional undersizing is intrinsic to the FFF process and mainly attributed to: (i) thermal shrinkage during material cooling; (ii) partial lack of interlayer consolidation and reduced effective wall thickness and (iii) slicing approximation, where the layer-by-layer discretisation of curved geometries leads to local rounding errors. The slightly higher dimensional accuracy of PLA_020 may be associated with the increased discretisation fidelity (more layers per unit thickness), which improves contour resolution. Conversely, PLA_028 benefits from improved thermal stability due to fewer thermal-cycle transitions per unit height, resulting in lower variability despite higher nominal undersizing.

The geometric deviation of the printed holes was quantified by analysing the roundness error. Fig. 9 shows the comparative box plot of the roundness values obtained for both layer thickness configurations and Table 2 shows the corresponding statistical parameters. Overall, the analysis revealed comparable roundness levels between the two PLA sample categories, with mean values of 0.2216 mm for PLA built with layer height of 0.20 mm and 0.2083 mm for PLA built with layer height of 0.28 mm, thus indicating limited influence of layer thickness on the circularity defect. However, PLA_028 exhibited a slightly smaller standard deviation and lower coefficient of variation (15.02%) compared to 18.11% in PLA_020, suggesting improved consistency and repeatability of the hole geometry when a thicker layer is adopted. This behaviour can be associated with the enhanced intra-layer bonding and reduced number of heat cycles occurring in PLA_028, which promote higher local thermal stabilisation during deposition. Conversely, the thinner layer provides finer geometric discretisation, but increases the frequency of deposition and cooling events, introducing higher variability.

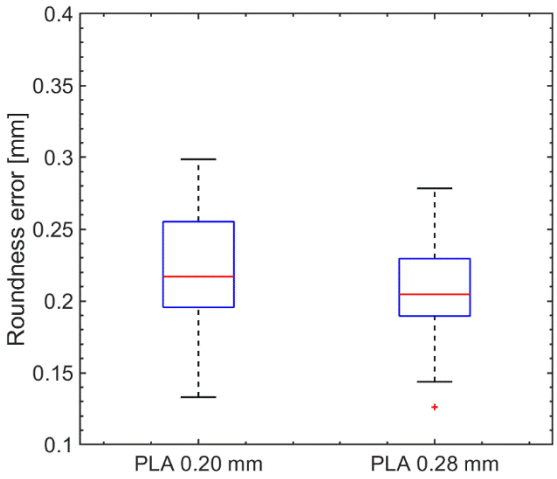

Fig. 9. Box plot of the roundness values obtained for both layer thickness.

Table 2. Roundness evaluation of AM-built holes obtained with different layer thickness configurations.

	PLA_020	**PLA_028**
Mean [mm]	0.22161	0.20827
St. dev	0.04014	0.03128
CoV [%]	18.11	15.02

Beyond the dimensional characterisation of AM-built holes, an analogous evaluation was carried out for the CNC-drilled counterparts. In this case, measurements were only taken under drilling conditions that produced minimal levels of burr and an acceptable quality of the internal surface of the hole. The LSC diameter was therefore evaluated exclusively for holes produced within the operational window previously identified as suitable in terms of burr formation (i.e., f = 0.05–0.10 mm/rev, and spindle speeds of 800 rpm for T-side drilling and 2400 rpm for B-side drilling). For T-side drilling, both PLA_020 and PLA_028 specimens exhibited their lowest burr levels at 800 rpm and 0.10 mm/rev. Under these conditions, the CNC-drilled holes showed near-nominal dimensional accuracy, with PLA_020 reaching an average LSC diameter of 6.348 mm (standard deviation 0.007 mm) and PLA_028 a mean value of 6.345 mm (standard deviation 0.009 mm). The dimensional deviation from the nominal tool diameter (6.35 mm) was therefore minimal (-0.002 mm and -0.005 mm, respectively). For B-side drilling, the smallest top burr was obtained at 2400 rpm – 0.10 mm/rev, whereas the most acceptable bottom burr occurred at 2400 rpm – 0.05 mm/rev, for both PLA_020 and PLA_028. Accordingly, LSC measurements were carried out at both parameter combinations. At 2400 rpm – 0.10 mm/rev, PLA_020 exhibited an average LSC diameter of 6.343 mm (st. dev. 0.010 mm), while PLA_028 stabilised at 6.339 mm (st. dev. 0.011 mm). At 2400 rpm – 0.05 mm/rev, values remained similarly close to nominal: 6.346 mm for PLA_020 and 6.341 mm for PLA_028, both with sub-0.012 mm standard deviations. Across all admissible conditions, the CNC-drilled holes consistently show dimensional errors $z < 0.01$ mm, with no meaningful difference between the PLA_020 and PLA_028 configurations. This stands in sharp contrast with AM-built holes, where LSC diameters were under sized by over 1 mm and exhibited significantly larger dispersion.

Conclusions

This study clarifies the fundamental differences between holes produced by fused-filament fabrication and those obtained through subsequent CNC drilling. Additively manufactured holes showed good repeatability but a systematic dimensional under sizing exceeding 1 mm relative to the nominal diameter. Both layer configurations (0.20 mm and 0.28 mm) displayed a quasi-Gaussian

dispersion of LSC diameter, confirming consistent process output but also revealing that FFF, in its native form, lacks the precision required for functional through-holes. Roundness deviations were also significantly higher than typical machining tolerances, and their magnitude was intrinsically linked to the staircase effect, layer morphology, and the thermal–geometric limitations of the slicing process. These results indicate that holes made with AM technology cannot be used as printed for applications requiring strict dimensional compliance, unless compensation or oversizing strategies are introduced during the design phase. In contrast, CNC drilling applied to AM components has been shown to restore near-nominal geometry, provided that the process parameters fall within the "acceptable for burr" operating window. When burr formation remains controlled (i.e., f = 0.05–0.10 mm/rev, and spindle speeds of 800 rpm for T-side drilling and 2400 rpm for B-side drilling), the resulting LSC diameters differ from the nominal value of 6.35 mm by less than 10 μm, with minimal variability. However, the work also shows that the interaction between the tool and the component introduces specific sensitivities depending on the combination of process parameters. Therefore, there is no single optimal combination; instead, it is necessary to adhere to a limited parameter window to balance primarily the thrust force (which affects tool wear) and minimisation of burr. Although this investigation was conducted on PLA using a single drilling tool geometry, the observed dimensional behaviour of the FFF holes is primarily determined by intrinsic process-related phenomena, such as layer deposition morphology, scale effect and thermal shrinkage. These mechanisms are common to most thermoplastics processed by FFF and therefore suggest that similar trends in terms of dimensional undersizing and deviation from roundness may occur in other polymers, although to an extent that depends on the material. On the contrary, the effectiveness of CNC drilling and the definition of an acceptable operating window depend on the thermomechanical properties of the specific polymer and the geometry of the drill bit used. Further investigations are therefore necessary, including different polymers and tool geometries, in order to quantitatively extend the window of identified parameters.

References

[1] Islam MA, Mobarak MH, Rimon MIH, Al Mahmud MZ, Ghosh J, Ahmed MMS, et al. Additive manufacturing in polymer research: Advances, synthesis, and applications. Polym Test 2024;132:108364. https://doi.org/10.1016/j.polymertesting.2024.108364.

[2] Su J, Ng WL, An J, Yeong WY, Chua CK, Sing SL. Achieving sustainability by additive manufacturing: a state-of-the-art review and perspectives. Virtual Phys Prototyp 2024;19. https://doi.org/10.1080/17452759.2024.2438899.

[3] Lalegani Dezaki M, Mohd Ariffin MKA, Hatami S. An overview of fused deposition modelling (FDM): research, development and process optimisation. Rapid Prototyp J 2021;27:562–82. https://doi.org/10.1108/RPJ-08-2019-0230.

[4] Solouki A, Aliha M, Makui A. A Methodology for Optimizing Impact Strength, Dimensional Accuracy and Costs of Manufacturing with Three-Dimensional Printing of Polylactic Acid. Arab J Sci Eng 2024;49:7545–69. https://doi.org/10.1007/s13369-023-08422-3.

[5] Pratheesh Kumar MR, Saravanakumar K, Arun Kumar C, Saravanakumar R, Abimanyu B. Experimental investigation of the process parameters and print orientation on the dimensional accuracy of fused deposition modelling (FDM) processed carbon fiber reinforced ABS polymer parts. Mater Today Proc 2024;98:166–73. https://doi.org/10.1016/j.matpr.2023.10.062.

[6] Zaborniak M, Bremek M, Budzik G, Kluczyński J. Analysis of the Dimensional and Shape Accuracy and Repeatability of Models Produced in the Process of Additive Extrusion of Thermoplastic Polymers Using Fused Filament Fabrication Technology. Applied Sciences 2024;14:6404. https://doi.org/10.3390/app14156404.

[7] Rebaioli L, Fassi I. A review on benchmark artifacts for evaluating the geometrical performance of additive manufacturing processes. The International Journal of Advanced Manufacturing Technology 2017;93:2571–98. https://doi.org/10.1007/s00170-017-0570-0.

[8] Gómez-Gras G, Pérez MA, Fábregas-Moreno J, Reyes-Pozo G. Experimental study on the accuracy and surface quality of printed versus machined holes in PEI Ultem 9085 FDM specimens. Rapid Prototyp J 2021;27:1–12. https://doi.org/10.1108/RPJ-12-2019-0306.

[9] Popescu D, Gheorghe Amza C, Marinescu R, Cristiana Iacob M, Luminiţa Căruţaşu N. Investigations on Factors Affecting 3D-Printed Holes Dimensional Accuracy and Repeatability. Applied Sciences 2022;13:41. https://doi.org/10.3390/app13010041.

[10] Chang D-Y, Lin C-H, Wu X-Y, Yang C-C, Chou S-C. Cutting force, Vibration, and Temperature in Drilling on a Thermoplastic Material of PEEK. Journal of Thermoplastic Composite Materials 2023;36:1088–112. https://doi.org/10.1177/08927057211052325.

[11] Lalegani Dezaki M, Mohd Ariffin MKA, Baharuddin BTHT. Experimental Study of Drilling 3D Printed Polylactic Acid (PLA) in FDM Process, 2021, p. 85–106. https://doi.org/10.1007/978-3-030-68024-4_5.

[12] Vishwadarshan, Shetty G, Shetty R, J P S, V B, Hegde A. Comprehensive analysis of drilling responses in additively manufactured PLA using a regression—based statistical learning approach. Mater Res Express 2025;12:055302. https://doi.org/10.1088/2053-1591/adcf7b.

[13] Panico M, Langella A, Boccarusso L. On the influence of clamping conditions and cutting edge geometry on drilling of thin aluminium stacks. CIRP J Manuf Sci Technol 2025;61:572–87. https://doi.org/10.1016/j.cirpj.2025.08.004.

[14] Panico M, Begemann E, Gebhardt A, Hartmann F, Herrmann T, Langella A, et al. Evaluating the impact of boundary conditions and clamping force in robotic one-up drilling of hybrid stacks. CIRP J Manuf Sci Technol 2025;60:1–14. https://doi.org/10.1016/j.cirpj.2025.04.003.

[15] Yaman U. Shrinkage compensation of holes via shrinkage of interior structure in FDM process. The International Journal of Advanced Manufacturing Technology 2018;94:2187–97. https://doi.org/10.1007/s00170-017-1018-2.

[16] Sajan N, John TD, Sivadasan M, Singh NK. An investigation on circularity error of components processed on Fused Deposition Modeling (FDM). Mater Today Proc 2018; 5: 1327-34. https://doi.org/10.1016/j.matpr.2017.11.218.

[17] Jiang Y, Wang X, Li H, Huang Y, Zhou Z. Experimental study for the effect of typical hole geometric deviation on film cooling effectiveness. Thermal Science and Engineering Progress 2026; 69:104446. https://doi.org/10.1016/j.tsep.2025.104446.